Tactile Discrimination Using Active Whisker Sensors

J. Charles Sullivan, Ben Mitchinson, Martin J. Pearson, Mat Evans, Nathan F. Lepora, Charles W. Fox, Chris Melhuish, and Tony J. Prescott

***Abstract*—We describe a novel, biomimetic tactile sensing system modeled on the facial whiskers (vibrissae) of animals such as rats and mice. The "BIOTACT Sensor" consists of a conical array of modular, actuated hair-like elements, each instrumented at the base to accurately detect deflections of the shaft by whisker-surface contacts. A notable characteristic of this array is that, like the biological sensory system it mimics, the whiskers are moved back-and-forth ("whisked") so as to make repeated, brief contacts with surfaces of interest. Furthermore, these movements are feedback-modulated in a manner intended to emulate some of the "active sensing" control strategies observed in whiskered animals. We show that accurate classification of surface texture using data obtained from whisking against three different surfaces is achievable using classifiers based on either naive Bayes or template methods. Notably, the performance of both these approaches to classify textures after training on as few as one or two surface contacts was improved when the whisking motion was controlled using a sensory feedback mechanism. We conclude that active vibrissal sensing could likewise be a useful sensory capacity for autonomous robots.**

***Index Terms*—Bayesian methods, biomimetics, classification algorithms, robotics, sensor systems and applications, tactile sensors.**

I. Introduction

An important characteristic of many biological sensory systems is that they are active, where "active" here means purposively controlled and information-seeking in the sense described by Bajcsy [1], rather than operating by emitting energy (which is an alternative meaning for the phrase "active sensing"). An example of biological active sensing, in the realm of touch, comes from the way we control the movement of our hands and fingers depending on the type of information about a surface or object of interest that is being sought. For instance, we typically stroke a surface with our fingertips to determine texture, palpate at different locations to judge shape, and press or squeeze to assess hardness [2]. In this paper, we discuss biomimetic tactile sensing in the context of a different, but perhaps equally important, active sensory system – the facial whiskers (or vibrissae) of mammals. Nearly all mammals have facial whiskers but the specialists in vibrissal sensing, such as rats and mice, tend to be creatures of small body-size living nocturnally, or in environments with limited natural light, who will use their whiskers in support of locomotion, navigation, prey catching, and even social behavior [3]. Vibrissal sensing is of interest to engineers as artificial vibrissae could provide proximal sensors that can determine distance to nearby objects alongside surface characteristics such as shape and texture [4]). A useful property is that vibrissal sensors could be employed in circumstances where the efficacy of other types of proximal sensing could be seriously compromised – for instance, in environments containing smoke or dust, or in darkness where there is a need to operate covertly.

The biomimetic vibrissal sensing system described in this paper has been developed as the result of a long-term collaboration between biologists and engineers aimed at advancing the understanding of biological vibrissal systems and determining to what extent, and in what forms, vibrissal sensing could be useful in engineered systems such as autonomous robots. Most recently, this collaboration has taken the form of a European Framework 7 project termed BIOTACT (BIOmimetic Technology for vibrissal Active Touch), and in this paper, we describe the design of a vibrissa-based sensory array – the BIOTACT sensor – that has been one of the chief focuses of that project. The BIOTACT sensor is the latest in a line of artificial vibrissal systems (see [4] and [5]) modeled most directly on that of the common rat. We have taken inspiration from this animal model in various ways, investigating and attempting to mimic aspects of: (i) vibrissal morphology including the physical characteristics of individual whiskers and their organization into a spatial-distributed array of different length elements; (ii) vibrissal control including the manner in which the whiskers are moved and positioned both through actuation of individual whiskers and through the ability to orient the full array; and (iii) vibrissal sensory processing including analysis of the types of tasks in which vibrissal sensing is employed by animals and the nature of the information they are thought to extract from vibrissal signals. In this paper, we consider each of these different areas of potential biomimicry. In each case, we briefly describe some of the salient characteristics of biological vibrissal systems, discuss how these have influenced the design of our artificial sensor, and show how the current sensor prototype implements key properties of interest. We also describe a number of experiments with this prototype showing, in particular, how we have implemented biomimetic vibrissal control, and how properties, such as surface texture and radial distance to contact, can be extracted from sensor signals. In the discussion, we consider the impact of active control on

Manuscript received November 19, 2010; revised March 31, 2011; accepted April 08, 2011. Date of publication April 29, 2011; date of current version December 07, 2011. This work was supported by the European Union FP7 BIOTACT Project (ICT-215910). The associate editor coordinating the review of this paper and approving it for publication was Prof. Raul Martin-Palma.

J. C. Sullivan, M. J. Pearson, and C. Melhuish are with the Bristol Robotics Laboratory, University of the West of England, Bristol, BS16 1QD, U.K. (e-mail: charlie.sullivan@brl.ac.uk; http://www.brl.ac.uk; martin.pearson@brl.ac.uk; chris.melhuish@brl.ac.uk).

B. Mitchinson, M. Evans, N. F. Lepora, C. W. Fox, and T. J. Prescott are with the Department of Psychology, University of Sheffield, Sheffield, S10 2TP, U.K. (e-mail: b.mitchinson@sheffield.ac.uk; Mat.Evans@sheffield.ac.uk; n.lepora@sheffield.ac.uk; charles.fox@gmail.com; t.j.prescott@sheffield.ac.uk).

Color versions of one or more of the figures in this paper are available online at http://ieeexplore.ieee.org.

Digital Object Identifier 10.1109/JSEN.2011.2148114

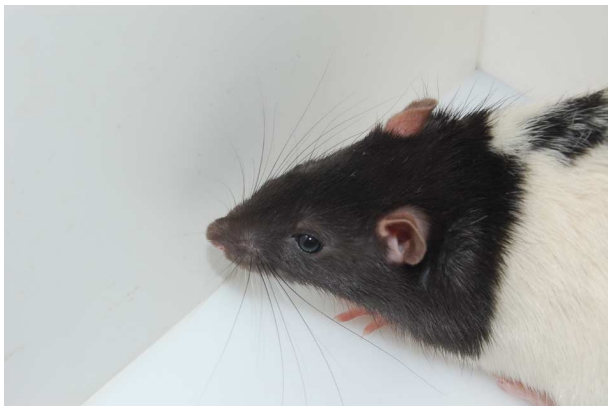

Fig. 1. Rat facial whiskers (*vibrissae*).

the information-gathering capacities of our novel sensor in the context of our twin goals of furthering the understanding of biological vibrissal sensing and developing useful artificial vibrissal sensors for robotics. Finally, we outline some of the limitations of our current sensor design and describe how these might be overcome in the future.

II. The BIOTACT Sensor

A. The Whisking System in Rat

Long facial whiskers, or *macrovibrissae*, are found in many mammalian species, projecting outwards and forwards from the snout of the animal to form a tactile sensory array that surrounds the head (see [6], and Fig. 1). In rats, the macrovibrissae form a two-dimensional grid of five rows on each side of the snout, each row containing between five and nine whiskers ranging between ~ 15 mm and ~ 50 mm in length. Each whisker is mounted in a specialized and mechanically complex hair follicle (see [7] for a description). These, in turn, sit within an area of dense muscular tissue strongly innervated by nerve fibers called the mystacial pad. From an engineering perspective, facial whiskers can be thought of as tapered elastic beams that deform easily upon contact with objects, and possibly also as the result of movement through air. Since the whisker shaft is composed of dead hair cells, the transduction of whisker deformations into neural activity begins inside the follicle where multiple populations of mechanoreceptors surround the base of the shaft and respond with high acuity when it is deflected. Mechanoreceptor responses are then transduced into patterns of neural firing in approximately 200 primary afferent fibers (per whisker) within the facial nerve. This transduction apparatus has been found to respond, in different ways, to rotation of the follicle by its muscles and deflection of the whisker shaft by external contacts. Thus, activity in facial nerve neurons is thought to encode information about the direction, velocity, and duration of whisker displacements.

When the rat is moving and exploring its surroundings the long facial whiskers are swept back and forth, at typical rates of seven to ten "whisks" per second [8]. The forward and backwards motion of each vibrissa is partly determined by its own intrinsic muscle, and partly by a set of extrinsic muscles that anchor the mystacial pad to the bones of the skull. Thus, although each whisker has some capacity for independent movement, the whiskers on each side of the snout generally move together, coupled by linkages within the pad and by the action of extrinsic muscles.

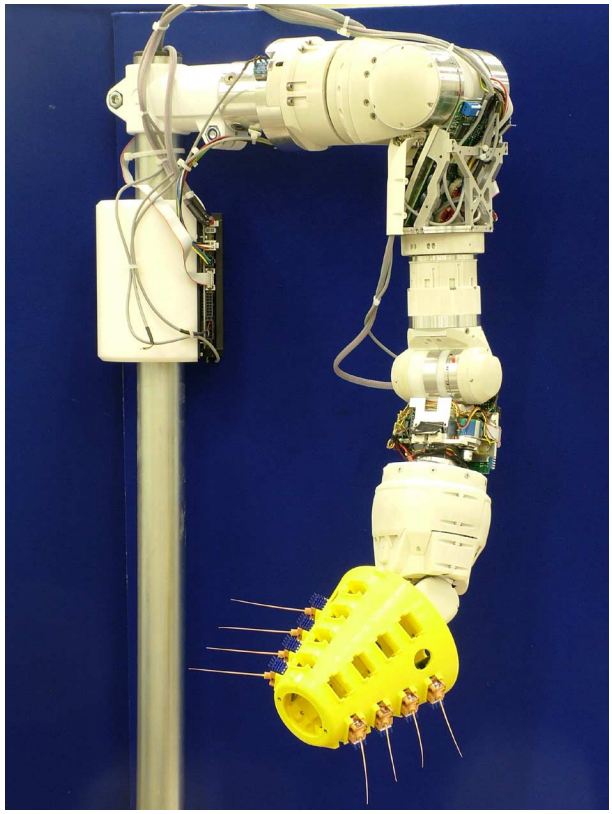

Fig. 2. The BIOTACT G1 sensor head and robot arm.

In addition to the macrovibrissae, rats also have a large number of shorter, more densely packed, and non-actuated microvibrissae on the chin and lips. These arrays of short whiskers are thought to form the "fovea" of the vibrissal system [9] being brought to bear on objects and surfaces by head and body orienting movements triggered when the longer whiskers make unexpected contacts.

B. Sensor Design

The Generation 1 (G1) BIOTACT sensor consists of a truncated conical "head" made from ABS plastic, which holds up to 24 whisker modules. The whisker modules are arranged in six radially symmetric rows of four and are oriented at outward-facing normals to the cone surface. For the purposes of our experiments and to enable accurate and repeatable location and movement of the sensor, it is mounted as the end-effector of a 7 degree of freedom robot arm (Fig. 2 shows the G1 sensor fitted with eight whiskers). Also, for the experiments reported here, the head was not fully populated with whiskers. Two rows were fitted with three whiskers each to create a bilaterally symmetric configuration.

C. Design of Active Whisker Sensor Module

The individual whisker sensors are completely modular in design, incorporating their own actuation mechanism and control electronics. Actuation is by means of miniature brushless DC motors (Faulhaber 1307BH), which incorporate an 11:1 gearbox, controlled by custom-built three-phase bridge drivers,

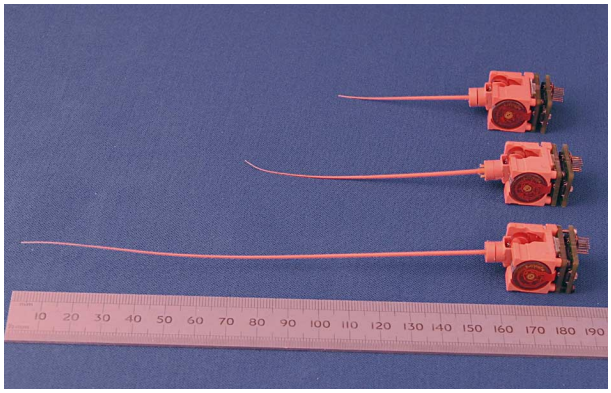

Fig. 3. Whisker modules.

with closed-loop PD control provided by on-board microcontrollers (Microchip dsPIC33FJ128GP802). The modules are 20 mm by 15 mm by 15 mm in size (see Fig. 3) and weigh 8 g including the controller boards. Typical power consumption during whisking is 0.9 W. They are capable of whisking at frequencies of up to 10 Hz, which is roughly comparable to the whisking rate of real rat mystacial whiskers [10].

Software to process the signals from the whisker sensors and to control the whisking patterns is written in C++ and executed under the BRAHMS Modular Execution Framework [11] on a PC which connects to the sensor head via a USB2 connection, running in high speed bulk transfer mode. This is able to transmit data to and from the sensor (half-duplex) synchronously at 500 μs intervals, enabling data transfer and feedback updates at 2 kHz.

The whisker sensor is based on the principle of Hall-effect detection of movement of a small magnet fixed to the base of the whisker. Monolithic triaxis Hall-effect sensor ICs by Melexis (MLX90333) are used and these incorporate two orthogonal pairs of Hall plates which, together with on-chip signal processing, enable the three orthogonal components of magnetic field strength, to be resolved with 14 bit resolution. These data, together with the protraction angle (θ) of the whisker relative to the head are sent in synchronous serial form using an SPI bus to the local microcontroller. Data from the microntrollers are collected via six separate SPI busses which are marshalled by an field programmable gate array (FPGA) (Xilinx Spartan 3e) and then sent to the first-in–first-out (FIFO) buffer of the USB controller (Cypress FX2). The FPGA acts as the bus master for the SPI busses and data transfers in packets of 512 bytes are synchronized with the USB2 host controller on the PC resulting in very low latency and jitter.

The whiskers are made using a Data Light Processing (DLP) rapid-prototyping machine (Envisiontec Perfactory) in Nanocure RC25, a composite material consisting of a UV-curing photo-polymer matrix and aluminium oxide nanoparticle filler. The combination of the DLP process and the composite material enable us to make whiskers which taper to a fine point (0.25 mm diameter) and yet retain sufficient strength and toughness to withstand repeated impact against the discriminanda. Two important benefits of whisker taper, and in particular the fine tip diameter were highlighted in [12]: a small tip should improve resolution of fine surface features (here, we are attempting to discriminate surface textures with mean particle diameters

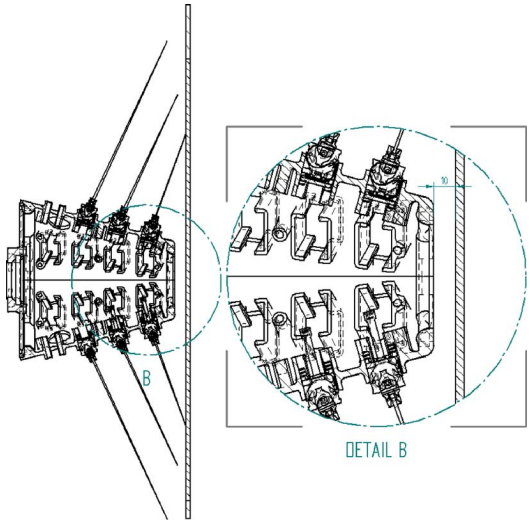

Fig. 4. G1 sensor in test configuration (section).

of 25 μm) and tip breakages (which are common for real rat whiskers) have a smaller effect on natural frequencies of vibration. The artificial whiskers have a taper ratio (hub/tip) of 8, whereas rat whisker taper ratios are typically 10–20 with tip diameters of ~ 10 μm. Rat whiskers are both tapered and curved but we have chosen not to mimic the curvature of the natural whiskers in these experiments. Future work will examine the effect that curvature has on the ability to discriminate texture.

Note also that the whisker lengths in the test configuration were not all the same: they increased from front to rear in order that all whiskers could touch a plane surface orthogonal to the axis of the cone (see Fig. 4). This feature was also motivated by the observation that the whiskers within each row of the mystacial pad of rats and other whisking mammals closely follow an exponential increase in length from the front to the rear: the actual ratio of length between adjacent whiskers is species and row specific, varying from 1.2 to 1.6 [9]. In our experiments, we used whiskers of length 80, 112, and 158 mm, corresponding to a ratio of 1.4. Our whiskers were longer than those of whisking mammals, which in rats are typically between 15 and 50 mm long [3]. The lowest static natural frequencies of vibration of the artificial whiskers were measured *in situ*, using Fourier spectral analysis of response after release from an imposed deflection parallel to the motor axis, as 86, 50, and 21 Hz, respectively. Frequencies of corresponding whiskers on each side were within 1 Hz. Studies of the mechanical characteristics of rat whiskers have revealed that they have natural frequencies in the same range. Hartmann *et al.* [13], for example, measured frequencies between 27 and 260 Hz, noting that in all cases whisker resonant frequencies were significantly higher than the whisking frequency.

III. Motor Control

A. Motor Control in Rats

Although early research emphasized the regularity and symmetry of whisker motion (e.g., [14]), more recent work by the current authors, and in other laboratories, has shown that biological whisker motion is often strongly modulated by the nature of the task [15], by the intentions of the animal [16], and by

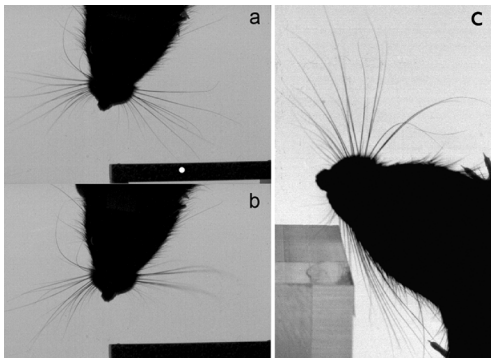

Fig. 5. Snapshots from high-speed videography recordings of rat whisker movement. (a) and (b) An example of rapid cessation of protraction (RCP). In (a), the left and right whisker fields are protracting synchronously when one of the forward whiskers in the ipsilateral (left-hand) field makes contact (indicated by the white dot) with a vertical surface. Protraction on the ipsilateral side ceased 12 ms later while protraction continued contralaterally (adapted from [17]). In (b), 32 ms after the contact, the ipsilateral whiskers are already considerably retracted when the contralateral field reaches maximum protraction. (c) An example of contact-induced asymmetry (CIA). Here, the whiskers ipsilateral (nearest) to the Perspex block can be seen to be considerably less protracted than those contralateral (image from the Active Touch Laboratory).

the immediate environment [17], [18]. It has been hypothesized (for example, see [17]) that some of these modulations are functional, and more specifically, that they are examples of "active sensing" control, serving to improve the quality and/or quantity of sensory information collected. The BIOTACT sensor is an ideal platform for testing these hypotheses: its great number of degrees of freedom allow the comparison of the impact of different motor control strategies on data collection. In the current paper, we focus on two candidate active sensing strategies, termed rapid cessation of protraction (RCP), and contact-induced asymmetry (CIA).

The forward and backward phases of the periodic "whisking" motions, observed in rats and mice, are usually denoted protraction and retraction, respectively. RCP is the observation that when the animal's whiskers encounter a novel object they often do so with a relatively "light touch"; that is, the forward protraction of the whiskers stops very soon (12–14 milliseconds) after the initial contact preventing strong bending of the whiskers against the surface. This was first observed by Mitchinson *et al.* [17] in the situation where the animal encounters an object on one side of the snout only (Fig. 5). Here, whisker motion on the ipsilateral (i.e., contacting) side of the snout can be seen to cease shortly after the contact, while protraction on the contralateral (opposite first contact) side continues seemingly unaffected by the surface impact. Grant *et al.* [18] went on to show that RCP takes place even when whiskers on both sides of the snout contact the surface and that it occurs in the second whisk cycle following the initial contact as well as in the first (and probably also in subsequent whisk cycles where there is continued contact). Interestingly, one effect of RCP can be to break the synchrony of the whisker movements in the left and right fields, potentially leading to extended periods where the whiskers on the two sides of the face move asynchronously (unpublished observations). RCP is an example of feedback control, since the sensory signals resulting from whisker-environment contact are used to regulate the same contact.

CIA is the related observation that when an animal has made contact with a nearby vertical surface the whiskers on the two sides of the snout are observed to move asymmetrically in subsequent whisks in advance of any further contact. Specifically, whiskers in the ipsilateral (nearest to surface) field tend to protract less, while the contralateral whiskers (furthest away) are seen to protract more strongly (Fig. 5). The result is, again, on the ipsilateral side, to allow the whiskers to make light contacts with the surface avoiding strong bending, while on the contralateral side the increased protraction tends to lead to more whisker contacts with the surface. CIA, in contrast to RCP, is an example of feed-forward control, since the sensory signals resulting from contact during one whisk are used to regulate contacts occurring during subsequent whisks.

Observationally, whisking behavior thus appears to be consistent with a 'minimal impingement, maximal contact' active control strategy [17], where "impingement" describes the extent to which the whiskers could be imagined to penetrate through the contacted surface if it were to offer no resistance. A further observed modulation of whisking, consistent with the maximal contact element of this hypothesis, has been described by Grant *et al.* [18]. This is the ability of the animal to differentially control the velocity of the forward and rear whiskers, and thus the angular separation or "spread" of the whiskers, in order to bring the rear whiskers further forward and (again) increase the number of contacts with the surface of interest.

In the following sections, we describe first our implementation of bilateral whisking pattern generation for the BIOTACT sensor using two coupled oscillators. We then describe how this is modulated by vibrissal signals to generate RCP and CIA that is functionally similar to that observed in the animal (N.B., we make no strong claim concerning the similarity of the underlying mechanisms). Although a number of active sensing strategies have been demonstrated on our earlier whiskered robot platforms [19]–[22], we have not previously investigated or measured the consequences of this active control for sensory discrimination. Our first efforts to do this using the BIOTACT sensor are described in Section IV.

B. Pattern Generation Model

Whisking, as described above, consists most simply of periodic forward and backward motion, and this is what we reproduce first using the BIOTACT Sensor. In the animal, it has been shown that the motion is generated by a Central Pattern Generator (CPG), an intrinsic oscillator that does not require connection to the environment to operate [14]. Since it is known that periodic whisking that is out-of-phase on the two sides of the animal may be expressed, at least two such oscillators must be present. However, whisking tends towards being in phase, so these oscillators must be coupled. In addition, the oscillators may be perturbed by extrinsic events.

We model two individual oscillators, each as a two-dimensional dynamical system with a time-dependent state Ψ_i. The state can be alternatively written as follows (time dependence is not explicitly shown in most of the equations below, for notational simplicity)

$$\Psi_i = \begin{bmatrix} \psi_{i,1} \\ \psi_{i,2} \end{bmatrix} = \begin{bmatrix} r_i \cos(\phi_i) \\ r_i \sin(\phi_i) \end{bmatrix}. \quad (1)$$

The subscript i is chosen from 1, 2 and indexes into the pair of oscillators (also denoted "left" and "right"). The update equation is given by

$$\frac{d\Phi_i}{dt} = D_i + C_i + P_i \tag{2}$$

where the three terms on the right-hand side represent the forcings due to, respectively, the oscillator characteristic, the coupling between the two oscillators, and any perturbation of the oscillator caused by extrinsic events. Integration is forward Euler with an integration period T and, for physical plausibility, all ψ states are hard limited to fall between plus and minus $\psi_{\lim} = 1.5$ after the computation of each timestep.

The update representing the dynamics is given in polar space for simplicity, as follows.

$$D_i^{\text{polar}} = \begin{bmatrix} \frac{(1-r_i)}{\tau_r} \\ 2\pi f_W \end{bmatrix}. \tag{3}$$

This represents a system with a limit cycle on the unit circle and a period of $1/f_W$ seconds. The whisking frequency is set to $f_W = 2$ throughout this report; we also define the whisk period, $T_W = 1/f_W$. Also throughout, we use $\tau_r = 2T_W$. The coupling forcing is given in Cartesian space, as follows:

$$C_i = \begin{bmatrix} \frac{(\psi_{j,1}-\psi_{i,1})}{\tau_{11}} + \frac{(\psi_{j,2}-\psi_{i,1})}{\tau_{12}} \\ \frac{(\psi_{j,1}-\psi_{i,2})}{\tau_{21}} + \frac{(\psi_{j,2}-\psi_{i,2})}{\tau_{22}} \end{bmatrix} \tag{4}$$

where $j = 3 - i$ is the index of the opposite oscillator and τ_{pq} is the time constant with which state $\psi_{i,p}$ is forced towards state $\psi_{j,q}$ of the opposite oscillator. Note that a negative τ_{pq} will tend to force states apart. In this report, only τ_{11} is not infinite (that is, only the first coupling term is nonzero), and it always takes a positive value of $2T_W$, which brings the oscillators back into phase with a time constant of one whisking period.

In this report, the only perturbation is a noise signal, given by the following:

$$P_i = \begin{bmatrix} \sigma_\eta H_{50}(\eta_{i,1}) \\ \sigma_\eta H_{50}(\eta_{i,2}) \end{bmatrix}. \tag{5}$$

$\eta_{i,d} \sim N(0,1)$ is White Gaussian Noise, H_{50} is a third-order low-pass Butterworth filter with 50 Hz cutoff frequency, and $\sigma_\eta = 0.005$ is a small noise amplitude. The first state of each oscillator, $\psi_{i,1}$, is associated with whisker protraction on that side by deriving a "muscle drive" signal from it as follows:

$$W_i = \frac{\tanh(2\psi_{i,1}) + 1}{2}. \tag{6}$$

The other state $\psi_{i,2}$ can be viewed as the recovery state of the oscillator, and its value does not affect any output. W_i is used to drive a mechanical model of the motion of the whiskers, as follows:

$$m\frac{d^2\theta_{i,w}}{dt^2} = q_{i,w}W_i - k\theta_{i,w} - \nu\frac{d\theta_{i,w}}{dt} \tag{7}$$

$m = f_W^2/100$ is a mass, $k = 1$ is a spring constant, and $\nu = 4\sqrt{km}$ a damping constant. Hence, $\theta_{i,w}$, the protraction angle of the wth whisker on the ith side, displays second-order dynamics in response to the muscle drive W_i. $q_{i,w}$ is the muscle gain (coefficient between drive and force) associated with the wth whisker on the ith side, and is given by the following equation:

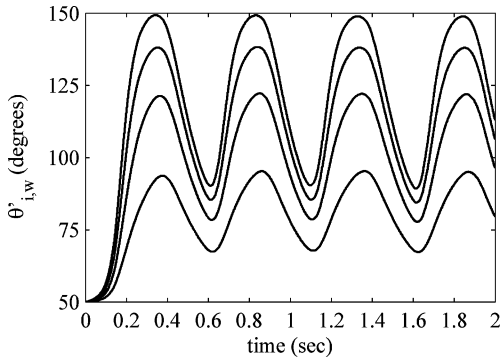

Fig. 6. $\theta'_{1,1}$ during free (unperturbed) whisking with four different values of $g_{1,1}$ (higher values generate higher values of $\theta'_{i,w}$).

$$q_{i,w} = 1.45(1 - z_i)g_{i,w}e^{-\theta_{i,w}^2} \tag{8}$$

$z_i \in [0,1]$ is a gating variable associated with the ith side. It takes a nominal value of zero (no suppression), and can range up to one (total suppression), modeling suppression of muscle drive to all whiskers on that side. $g_{i,w} \in [0,2]$ is a gating variable associated with the wth whisker on the ith side, which controls how excitable the individual whisker is – i.e., how much the whisker responds to the drive from the oscillator. It takes a nominal value of one, and can range both positively and negatively, modeling excitation or suppression for each whisker individually. The constant term scales the overall gain so that with $z_i = 0$ and $g_{i,w} = 2$, θ approaches, but does not exceed, unity (see below). The final (exponential) term is a simple model of the reduction in force produced by a muscle as its length decreases (reaching 37% as θ reaches its maximum value of unity). The overall effect is that the values of z_i and $g_{i,w}$ control the response of each side and each whisker, affecting both amplitude of oscillation and mean protraction angle, although it should be noted that there is no direct independent control over these latter variables.

An example of the effect of varying the gain is given in Fig. 6. The output, the angle of the first whisker on the left side, is given for $z_1 = 0$ and $g_{1,1} \in \{0.5, 1.0, 1.5, 2.0\}$. $\theta' = 100\theta + 50$ is plotted, which is the conversion of θ (which ranges in zero to one) into an angle in degrees to pass to the motor hardware.

C. Rapid Cessation of Protraction

A substantial component of whisker motor control that has been quantified is the *Rapid Cessation of Protraction* (RCP) that often follows contact between the whiskers and the environment, and which is hypothesized to limit the degree to which the whiskers bend during contact [17], [18]. We wish to reproduce this aspect because controlling the degree of bending could potentially improve the quality of data collected.

A contact signal is derived on each side from the x-deflection of the whiskers on that side (contact usually elicits strong x-deflection since the sensory x axis is parallel to the actuated axis).

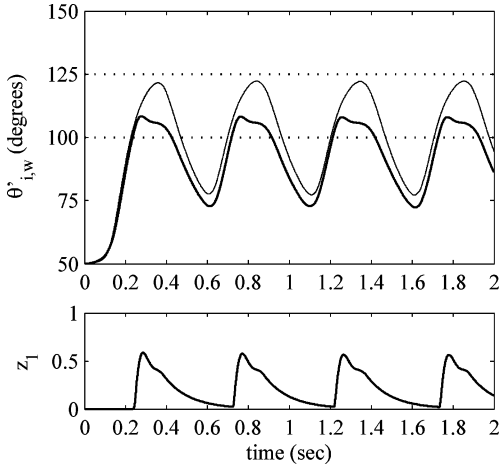

Fig. 7. Whisking with RCP modulation. When the left whiskers (thick line) are driven past a simulated obstacle (lower dotted line), a contact signal results which temporarily excites the gating variable z_1 and suppresses protraction ipsilaterally. The right whiskers (thin line) do not reach the obstruction on that side (upper dotted line), and are not modulated (thus, they show the expected movement of the left whiskers if the modulation were absent).

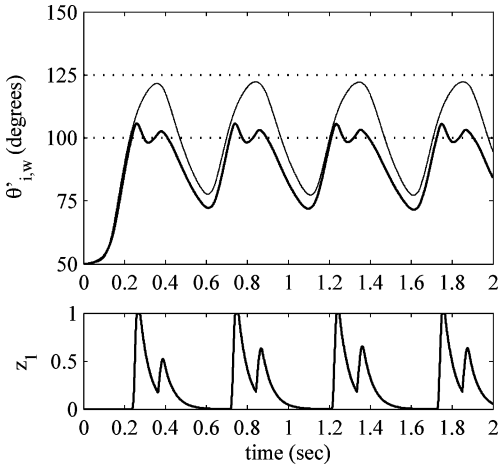

Fig. 8. Whisking with strong and fast RCP modulation. Left whiskers (thick line) quickly detach from the simulated obstacle (lower dotted line), and protraction reignites within a single whisk, leading to a biphasic whisk profile and two distinct contacts with the obstacle. The movement of the right whiskers (thin line) shows the expected movement of the left whiskers if the modulation were absent.

A third-order low-pass Butterworth filter with 50 Hz cutoff frequency H_{50} is first used to smooth the noisy whisker sensory signals. The maximum absolute value of this signal, across all whiskers on a side, forms the contact signal, π_i

$$\pi_i(n) = \max_{w\in[1,12]} \left| H_{50}(x_{i,w}(n)) \right|. \tag{9}$$

This signal is used to suppress protraction ipsilaterally, through the gating variable z_i, without affecting the oscillator dynamics. The gating variable dynamics are given by

$$z_i(n) = \left\langle \max\left(\left(1 - \frac{T}{\tau_z}\right) z_i(n-1), \sigma_z \pi_i(n) \right) \right\rangle_0^1 \tag{10}$$

where σ_z is a gain associated with the motor modulation, and $\langle\,.\,\rangle_a^b$ is a limit operation (transforming values not in the interval $[a, b]$ onto the nearest value that is in the interval). Contact on any whisker, thus, suppresses protraction ipsilaterally, an effect which decays with time constant τ_z. We can simply simulate contact signals from the whisker sensors using the following equation:

$$x_{i,w} = \left\langle \sigma_x \max\left(0, \theta'_{i,w} - \theta'_{i,\lim}\right) \right\rangle_{-1}^{+1}. \tag{11}$$

We simulate an obstruction at a different location on each side by setting $\theta'_{1,\lim} = 100$ and $\theta'_{2,\lim} = 125$, using $\sigma_x = 0.1$. Setting $\sigma_z = 0.7$ and $\tau_z = T_W/4$ generates the results graphed in Fig. 7. Protraction on the contacting (left) side is suppressed during contact, such that the depth of contact is controlled. The oscillator dynamics are unaffected, so the phase behavior is unchanged. Furthermore, the gating variable z_1 has all but recovered by the time of the next contact, so there is no inter-whisk modulation; that is, this aspect of control is entirely *reactive*.

We can simulate stronger and faster RCP control by setting $\sigma_z = 2$ and $\tau_z = T_W/10$; the results are shown in Fig. 8. In this case, protraction is more strongly suppressed such that the $\theta_{1,w}$ quickly fall below $\theta_{1,\lim}$ and the contact signal π_i becomes zero. Thus, the gating variable z_1 quickly recovers, and protraction reignites within the same whisk period, resulting in a biphasic whisk profile. We hypothesize that this control loop may be the origin of the biphasic whisks that have been observed in whisking animals [23].

Note that in the experiments presented in Section IV, we have set τ_z to $T_W/4$ throughout and the maximum value of σ_z was 0.9 so that this biphasic whisking was not encountered.

D. Contact-Induced Asymmetry

Another aspect of whisker motor control that has been measured is *Contact-Induced Asymmetry* (CIA), in which contact with a unilateral obstruction has been shown to reduce/increase whisker protraction on the ipsilateral/contralateral side [17], [18]. Here, we model CIA by introducing global excitation of protraction in all whiskers following contact, through the gating variables $g_{i,w}$. CIA results from the interaction of this global excitation with the reduction of protraction on the ipsilateral side due to the RCP mechanism described above.

The dynamics of $g_{i,w}$ are governed by the equations below. The results of using this modulation with $\sigma_g = 0.5$ and $\tau_g = T_W/4$ ($\sigma_z = 0.7$, $\tau_z = T_W/4$, as for Fig. 7) are shown in Fig. 9. The whiskers on the right side are now brought forward and "find" the obstruction

$$g_{i,w}(n) = \left\langle \max\left(g^*_{i,w}(n), \sigma_g \zeta(n)\right) \right\rangle_0^2 \tag{12}$$

$$g^*_{i,w}(n) = g_{i,w}(n-1) + \frac{T}{\tau_g(1 - g_{i,w}(n-1))} \tag{13}$$

$$\zeta = \max(\pi_1, \pi_2). \tag{14}$$

E. Summary

In summary, the motor control strategies described in this section may help the robot, in emulation of the rat, to take best advantage of its sensors (whiskers) in the face of the changing geometry of its near environment (Figs. 5 and 9). Complete quantification of the impact of these strategies in different sensory tasks will require extensive testing. In the following section, we

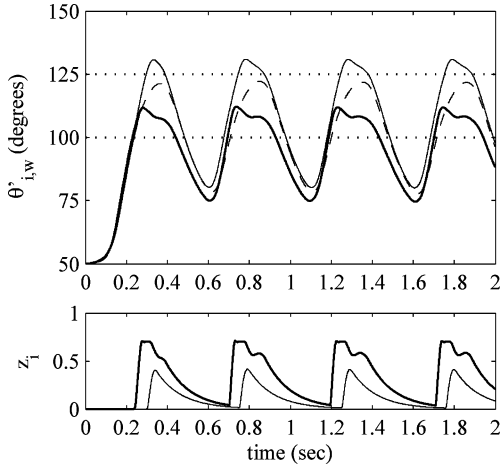

Fig. 9. As Fig. 7, but with CIA modulation enabled as well as RCP modulation. The left whiskers (thick solid line) contact an obstruction (lower dotted line) first, and cause excitation of the gating variables $g_{i,w}$, leading to global excitation of protraction. Thus, the right whiskers (thin solid line) are pushed forward and "find" the obstruction on the right side (upper dotted line) – compare with Fig. 7, where the obstruction on the right side is not found. Since both sides are modulated, here, we show also (dashed gray line) the expected movement of both sides were the modulations absent.

present our first assessment of the impact of implementing RCP, measuring the effect on performance in a texture discrimination task.

IV. Sensory Discrimination

A. Sensory Discrimination in Rats

Experiments with rats (reviewed in [3] and [24]), and with other tactile specialists such as the Etruscan shrew [25], have shown that whiskered animals are able to use their facial vibrissae to localize objects in space and to discriminate object properties such as shape and texture. For instance, in localization tasks, rats have been shown to use vibrissal information in gap measurement and gap jumping, and to be able to measure angular position of a contact along the sweep of the whisker, and the axial distance to a point of contact on a single whisker. Ahissar *et al.* [26] have proposed that the timing and extent of bending of the whiskers together provide sufficient information to localize a point of contact in three-dimensional space (elevation, azimuth, and axial distance, respectively). Several studies have shown that rats can use their macrovibrissae to reliably discriminate between surfaces with different texture, showing a similar level of acuity to human fingertips [10], [27], [28]. Movement of an individual whisker across a texture has been shown to give rise to a characteristic whisker vibration or "kinetic signature" which is thought to form the basis on which sensory discriminations are made [24], [29], [30], although the precise process that underlies such discriminations is not well understood.

A number of studies with artificial whiskers have looked at classification or feature detection tasks that require tactile discrimination abilities similar to those seen in whiskered animals. Previous work is this area has been reviewed by Fox *et al.* [5] and Prescott *et al.* [4]. In the current study, we sought to examine the capacity of the BIOTACT sensor to simultaneously extract two different stimulation parameters: the horizontal (axial) distance to the contacted surface and the texture of that surface, with and without whisking modulation using RCP. To evaluate the effectiveness of the BIOTACT sensor in this discrimination task, we tested two different classification methods that we have developed for use with artificial vibrissal signals, one template-based [5], [31], [32]), the other using "naïve" Bayes [33], [34]). Here, we describe the experimental setup used to generate a $3 \times 3 \times 3$ (axial distance, texture, RCP) training, and test (validation) datasets. We then briefly describe the two classification algorithms and the results of applying these to the BIOTACT sensor data.

TABLE I
Textured (Abrasive) Surfaces

ISO Grade	average particle diameter (μm)
P240	58.5
P600	25.8

B. Texture Classification Experiments

A set of textured surfaces were fixed in a vertical plane and rigidly attached to the robot arm's support post. The arm trajectory was preprogrammed to bring the front of the sensor to within a specified horizontal axial distance from the surface (5, 10, or 15 mm) with the two rows of whiskers aligned in a horizontal plane. Fig. 4 shows a horizontal section through the sensor in its test configuration. All experiments were carried out with a whisk frequency (f_W) of 2 Hz. This is somewhat slower than the whisking frequency of rats (dominant frequency 8 Hz [10]), but this is not unreasonable given the greater length of our whiskers (see Section II-B). The choice of the 2 Hz frequency is fairly arbitrary, however, and limited testing at other whisking frequencies has not revealed that this parameter is critical in achieving successful texture classification.

Three different textures have been used as discriminanda, a smooth plastic surface and two grades of commercial abrasive (3M silicon carbide "Wetordry Tri-M-ite") see Table I. The latter surfaces were chosen to give a direct comparison with the whisking mobile robot "Whiskerbot" texture classification reported by Fox *et al.* [5].

The combination of three distances and three textures gave a total of nine distinct classes to be discriminated between.

We also present results comparing three different whisking strategies.

— **Unmodulated**.
The whisker pattern generator output, unperturbed by feedback from sensors.

— **RCP7**.
Motor drive signal modulated with RCP, using a moderate gain factor [$\sigma_z = 0.7$, see (10)].

— **RCP9**.
Motor drive signal modulated with RCP, using a stronger gain factor [$\sigma_z = 0.9$, see (10)].

The purpose of this experiment was to determine whether RCP modulation was effective in improving the accuracy and robustness of classification and not to determine optimal values of

these parameters. As such, we chose values which we knew would be large enough to have a clearly visible effect on the output waveforms and small enough to prevent the biphasic whisking effect seen in simulation in Fig. 8.

C. Stationary Naïve Bayesian Classification

Bayesian classification involves recording the likelihoods of measurements from example sensory data. Given new test data, these likelihoods are used with Bayes' rule to calculate the posterior probability of the test data being drawn from each trained class. The class with the largest posterior is most probable.

Here, a stationary naïve Bayes classifier was used that had previously been demonstrated as an effective classifier of texture data [33], [34]. A naïve version of Bayes' rule, in which the measurements are assumed to be statistically independent is used, along with an assumption of identical likelihoods over time, to calculate the posterior probability for each class of training data.

Briefly, the training data is used to estimate the log-probability distributions $\log P_w(x_i|\mathrm{C}_l)$ (log-likelihoods) of each sensor measurement x_i occurring. Measurements were quantized into one hundred equal-width intervals that spanned the entire data range of each whisker, then the resulting histogram of sensor measurements smoothed with a Gaussian of width 5 intervals to correct for sampling errors and normalizing by the number of samples to give the likelihood. This led to $n_w \times n_C$ log-likelihood functions, for each of the $n_w = 12$ whisker inputs (two sensor directions for each of the six whiskers) and $n_C = 9$ texture/distance classes.

Then, for each validation trial, the classification was achieved using naïve Bayes rule to calculate the nine posterior probabilities for each of the texture/distance classes, representing that the measurements were drawn from the 12 likelihoods for each of these possible classes. These posterior probabilities were calculated from the stationary naïve Bayes' rule

$$\log P(\mathrm{C}_l|x_1,\ldots,x_n) = \sum_{w=1}^{12}\sum_{i=1}^{n} \log P_w(x_i|\mathrm{C}_l). \tag{15}$$

for flat priors, a stationary likelihood and the "naïve" assumption of statistical independence. The classification is given by the largest log-posterior for each validation trial,

$$\mathrm{T} = \arg\max_{\mathrm{T}_l} \log P(\mathrm{C}_l|x_1,\ldots,x_n). \tag{16}$$

The utility of the stationary naïve Bayes rule is that it greatly simplifies the process of calculating the posteriors to an algorithm that is linear sum over log-likelihoods. Then, the classification is similar in algorithmic complexity to a linear perceptron. Hence, the classification is extremely fast, with real-time performance easily achievable on a standard PC.

D. Sum-of-Squares Template-Based Classification

Template-based classification involves recording example sensory data as templates during a training phase, and comparing the stored templates to new data during the test phase. A template-based classifier has been shown to be successful in discriminating whisker contacts of varying radial distance and speed [31]. Template-based classification involves recording example sensory data as templates during a training phase, and comparing the stored templates to novel data during the test phase. By systematically comparing the novel data to signals encountered previously, a classification can be made by declaring which of the stored templates the novel signal is most similar to. This approach is straightforward to implement, and requires very little computation or preprocessing of the signal.

It has been shown previously that texture discrimination is dependent on whisker movement [35], and surface position [5]. In the present study, each template corresponds to a texture-distance pair. Classification based on these templates is, therefore, simultaneous classification of both the texture and distance to contact. From the training dataset, an array of templates were generated by storing the average of the signals for each whisker in each class in the training set. This gave rise to 9 sets of 12 templates. During the test phase, trials were taken at random from the test set as inputs to the classifier. An element-wise sum of squared errors calculation was made between the input I and each template T_i

$$e(T_i) = \sum_{t=1}^{n} (I(t) - T_i(t))^2 \tag{17}$$

where n is the length of the template, in samples. A sum of errors from the 12 templates in each set were taken, and compared across the 9 classes. The class with the lowest total sum of squared errors was determined the winner, and a recording was made in an output array of the estimated texture and distance to contact of the input trial.

E. Classification Performance

1) Overall Classification Performance (Unmodulated Whisking Dataset): The hit rates over multiple validation trials were first calculated for the unmodulated whisking dataset. From one to eight training whisks were used. Because a total of 12 (training and validation) whisks were measured, from 11×9 to 4×9 single whisks remained for validation over all nine texture/distance classes. The hit rate for each whisk number was then plotted against the number of training whisks [Figs. 10(a) and 11(a), solid black lines]. Both classifiers show classification accuracy increasing with numbers of training whisks and reaching a maximum after 4 or 5 training whisks. Thereafter, increasing the number of whisks leads to similar performance.

2) Comparative Performance of Unmodulated Whisking, RCP7 and RCP9 Datasets: The unmodulated whisking dataset discussed in the preceding study was compared with results from the RCP datasets. Hit rates for each whisk number are plotted in Figs. 10(a) and 11(a), dashed and dotted lines.

For both classifiers, the RCP modulated whiskers give higher hit rates after one or two training whisks than the unmodulated, with RCP7 giving the highest accuracy. However, the two classifiers behave differently as the number of training whisks increases; using the stationary Bayesian method RCP7 continues increasing, reaching 100% accuracy after seven training whisks,

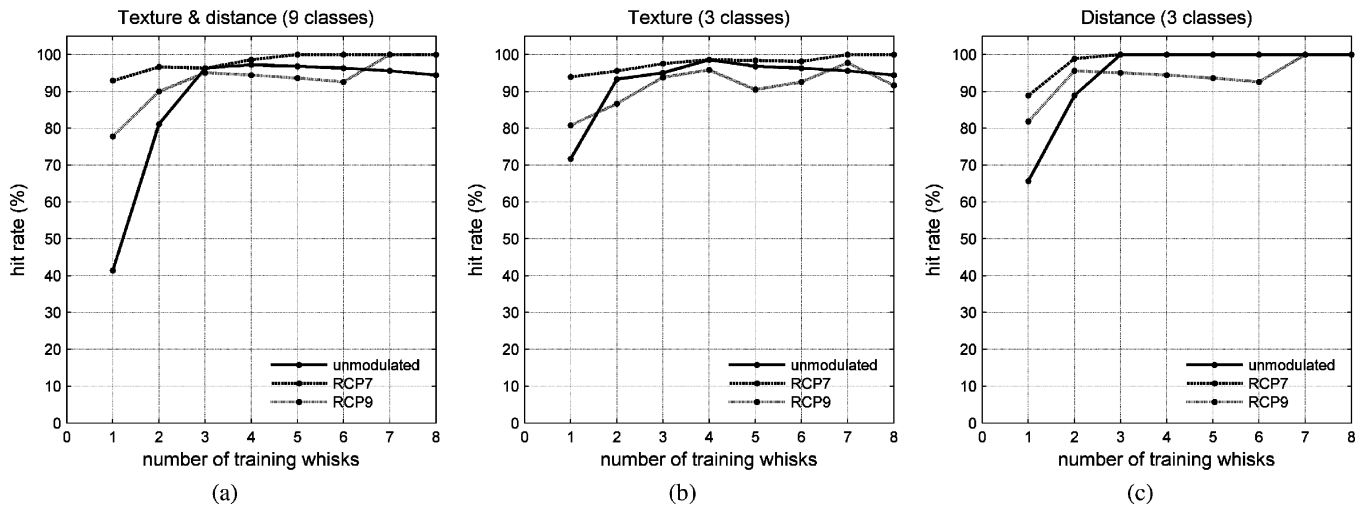

Fig. 10. Classification performance using naïve Bayes. Panel A compares the performance of the unmodulated, RCP7, and RCP9 datasets for classifying both texture and distance together. Panels B and C are analogous to panel A, but for a single classification of either texture or distance. Classification accuracy is measured by hit rate, which is the ratio of successful classifications to validation whisks. (a) Combined texture and distance. (b) Texture classification. (c) Distance classification.

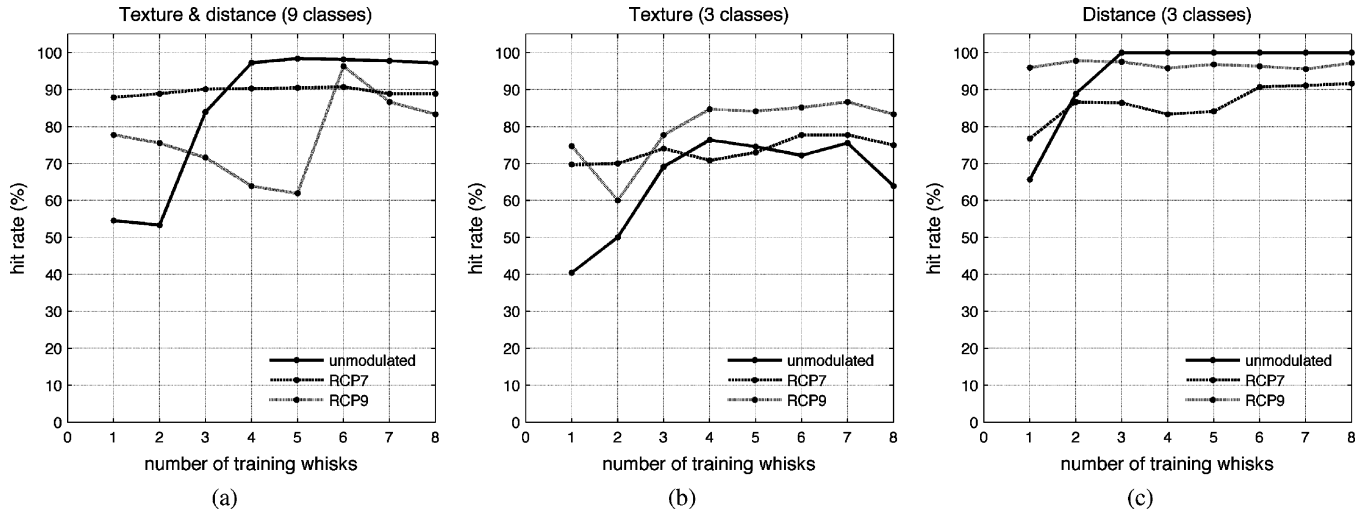

Fig. 11. Classification performance using template based classifier. Classification accuracy is measured by hit rate, which is the ratio of successful classifications to validation whisks. (a) Combined texture and distance. (b) Texture classification. (c) Distance classification.

whereas with the template classifier, RCP7 shows little improvement and RCP9 begins to lose accuracy with increased training but suddenly improves after six training whisks.

3) Classification Performance for Just Textures or Distances (Unmodulated Whisking Dataset): Classifiers for texture or distance (three classes of each) were then constructed by concatenating all training data for each distance or each texture. (Equivalently, the likelihoods could be averaged.) Once again, the number of training whisks was varied from one to eight and the hit rates plotted against whisk number [Figs. 10(b) and (c) and 11(b) and (c) solid lines].

Using the stationary Bayesian method, classification for both features again reached high accuracy after about three/four training whisks. Roughly speaking, the hit rate for the single classifier texture/distance classifier was about equal to multiplying the hit rates for the individual classifiers, so there was no advantage apparent from considering either the single nine-class method or the double three-class methods to distinguish both texture and distance. It should be noted that the double method is more efficient computationally, because a total of six classes are considered rather that nine.

The template-based method performed similarly on the distance classification task but only reached 75% hit rate on the texture classification.

4) Comparative Performance for Just Textures or Distances of Unmodulated Whisking, RCP7 and RCP9 Datasets: Finally, the single-classifiers of texture or distance were applied to the RCP7 and RCP9 datasets and the hit rate plotted against training whisk number [Figs. 10(b) and (c) and 11(b) and (c) dashed and dotted lines].

With the stationary Bayesian method, the same pattern of RCP7 being the best classifier, followed by RCP9 and then unmodulated whisking was again found, with the classification performance reaching its maximum at four whisks.

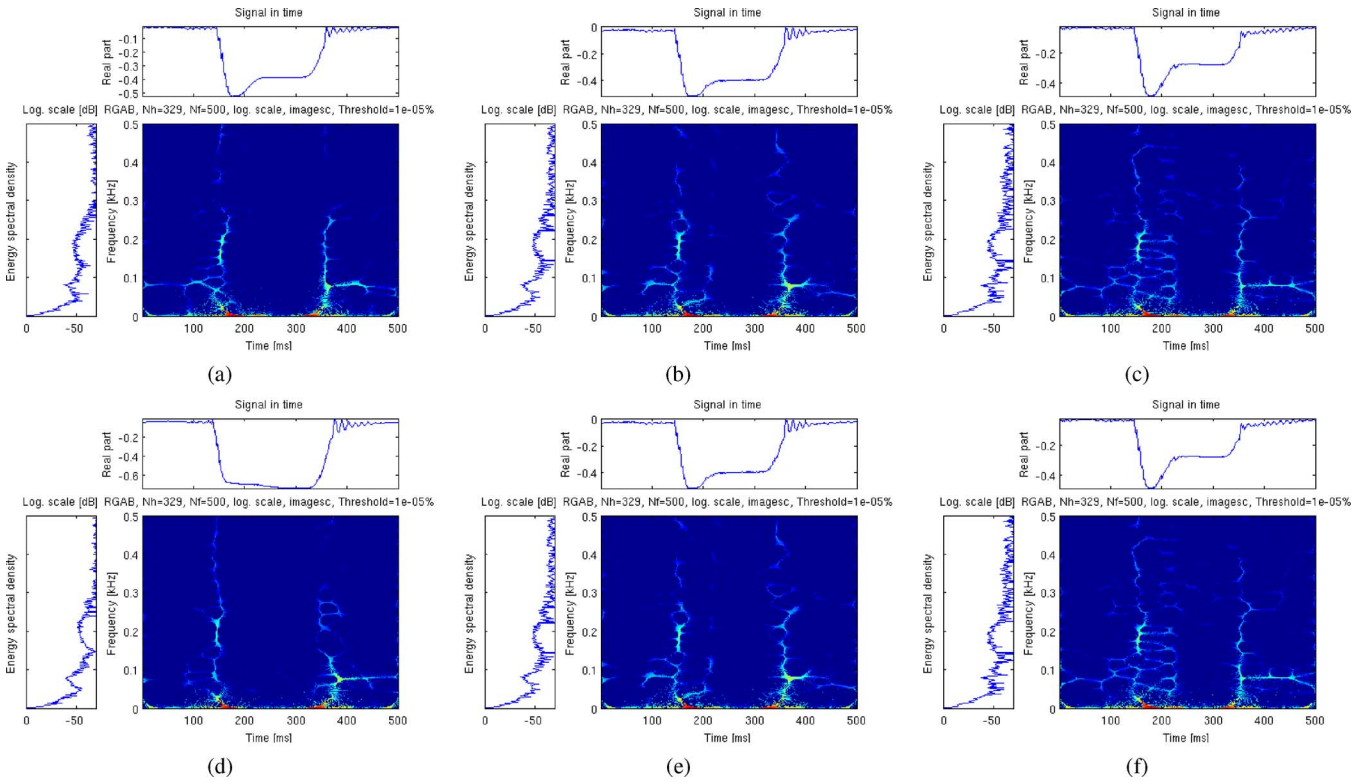

Fig. 12. Spectral analysis comparing response of smooth and textured (p240) surfaces with and without RCP modulation. Spectrograms computed using reassigned Gabor time-frequency representation [Time Frequency Toolbox (http://tftb.nongnu.org) *tfrrgab* function]. (a) Unmodulated, smooth. (b) RCP 0.7, smooth. (c) RCP 0.9, smooth. (d) Unmodulated, p240 abrasive. (e) RCP 0.7, p240 abrasive. (f) RCP 0.9, p240 abrasive.

With the template-based method, RCP9 gave higher classification accuracy in texture classification. This was also the case in distance classification with less than three training whisks, but RCP modulated whisking resulted in lower accuracy than unmodulated with more training contacts.

V. Discussion

The design of tactile sensor systems for robots has taken inspiration from mammalian whiskers (see [4]), and from insect antennae (see, e.g., [36] and [37]), since at least the 1980s. However, most work in this field has not specifically addressed the contribution of sensor motion to the problem of tactile discrimination. Earlier work by the current authors identified characteristic features of active sensing control in the whisker movement of rats [17], [18] and showed that these could be incorporated into artificial vibrissal systems for robots [20], [21]. In the current study, we extended this work to directly examine the impact of active control on a two-dimensional (texture $\times$ distance) sensory discrimination task. Based on these early results, we appear to see an advantage for active control (rapid cessation of protraction – RCP) for classification after fewer training whisk cycles, particularly when using the stationary naïve Bayes method. This outcome is perhaps surprising in that RCP tends to reduce rather than increase the duration of contact between the whisker and the surface. It therefore suggests that the benefit of RCP may be to increase the repeatability of whisker-surface contacts. The advantage is not clearly demonstrated when using the template-based method and more than two training whisks; under which circumstances classification of distance was actually less accurate when RCP modulation was applied. Further experiments both with artificial vibrissae and perhaps, using *in vivo* electrophysiology in animals, could usefully investigate the specific consequence of this aspect of control that might lead to improved discriminative capabilities. One of the advantages of the BIOTACT Sensor, over our earlier work on artificial vibrissal systems, is that the whiskers are individually actuated; therefore, sensor movement can potentially be modulated by sensory feedback on a per-whisker basis. Although we have yet to explore this possibility, our experimental work with rats suggests that whisker velocity can be differentially controlled for more anterior and posterior whiskers in a manner that affects the angular spread of the whiskers [18]. We also found a difference of up to 5 milliseconds in the timing of RCP, with posterior whiskers beginning to retract later than more anterior ones [18]. The artificial whisker results presented above suggest that such differences, while subtle, could be impacting on the discrimination capabilities of the whiskers. Since the experiments described here used only symmetric contacts with a vertical surface, we have also yet to investigate or quantify the impact of other aspects of active whisking control (particularly contact-induced asymmetry) on sensory processing.

It has been shown previously that whisker-based texture discrimination is critically dependent on whisker-object contact geometry [5]. In the current study, inspection of the raw signals for each class reveals greater within class variation for contacts with a given texture than at a given distance. This is because contacts at different distances result in stereotypical macroscopic changes in whisker deflection amplitude [32], whereas texture-dependent features involve smaller and more variable deflections of the whisker (either by their direct contact with random

particles on the rough surface or by an oscillatory "ringing" of the whisker as it draws away from the surface). This variation could perhaps explain why the template-based classifier considered here did not generalize well across conditions when attempting to classify texture, compared to the stationary Naïve Bayes classifier [compare Figs. 10(b) and 11(b)).

Fig. 12 shows single-whisk time histories of the signals from one of the smaller whiskers contacting the smooth and p240 textures at the same distance, together with spectrograms computed using the reassigned Gabor time-frequency representation [38]. Although the effect of RCP can be clearly seen in the time history, the differences between textures are more subtle.

Further support that the time-independence of a classifier can lend its robustness in certain circumstances is given by an equivalence between the template classifier and a form of Naïve Bayes classifier. Because the considered template classifier uses a sum-of-squares error function, it is equivalent to a log-product of independent noise terms that satisfy the Naïve Bayes definition

$$\sum_{t=1}^{N}(I(t)-T_i(t))^2 = -\log\prod_{t=1}^{N}\frac{1}{Z_i}\exp-\frac{(I(t)-T_i(t))^2}{2\sigma^2} - c \tag{18}$$

for constants $\sigma = 1/2$, $c = \sum_i \log Z_i$, and Z_i area-terms canceling with c. We can then consider the differences between these two forms of Naïve Bayes. The above Naïve Bayes formulation of the template classifier assumes varying noise distributions over time t and can thus be interpreted as a time-dependent Naïve Bayes classifier. In contrast, the Naïve Bayes considered earlier in this paper was stationary, supporting that time-dependence/independence is the principle difference between the two classifiers considered here. That being said, in some circumstances the simplifying assumption of time-independence may be a hindrance, for example, when the phases of the oscillations are crucial to the classification. Future work could investigate new forms of Naïve Bayes rules combining useful properties of both methods. The success of Naïve Bayes classification is encouraging and suggests that this relatively simple technique could potentially be a useful tool for other discrimination tasks involving time series data.

One of the goals in designing this first generation BIOTACT Sensor was to produce a modular unit that could be flexibly assembled into different configurations. The first configuration investigated was chosen to be a simple, radially symmetric cone with a small number of whiskers. This configuration clearly does not match the vibrissal system of the rat in a number of ways, one important consequence of which is that the sensory "surface" formed by the whiskers tips at full protraction does not form a broad field in front of the sensing device in the manner observed in animals (compare Figs. 1 and 2, for example). A second generation system, currently under construction, is being developed to specifically address this limitation. It will also incorporate an array of shorter, more closely spaced, unactuated *microvibrissae*, again based on the morphology of the rat which has a similar array on the frontal part of the snout and around its mouth and which have been shown to play a key role in object discrimination [9]. In addition to a more biomimetic sensor morphology, we also plan to improve aspects of the sensory processing. For instance, we have shown that, in the task of detecting whisker-surface contacts, sensor noise, due to the movement of the whiskers alone, can generate spurious false positives [39]. To address this problem, we previously developed an adaptive filtering algorithm that uses a copy of the motor control signal to predict movement-related sensory noise, such that cleaned-up signals (from which the predicted noise is subtracted) avoid the problem of spurious contacts. The same filter will likely prove useful in discrimination tasks such as the distance/texture problem considered above. Interestingly, the algorithm employed for adaptive filtering was modeled on the microcircuitry of the mammalian cerebellum, which, in rats, is known to be heavily involved in processing vibrissal signals.

A long-term ambition of our research is to identify the computations that are carried out in the rat brain when the animal is engaged in tasks that involve tactile discrimination. The classification methods, described above, are not specifically derived from considerations of how vibrissal processing mechanisms in the rat brain may operate. However, if we are able to devise effective classifiers whose capabilities match those of the rat, these can, in the future, be used to inform hypotheses about the biological system that may be testable using neurophysiological data.

Most tactile sensors for robots are binary devices that do little more than detect whether or not a contact has happened. Biology shows us that this is a modality with considerably greater potential. In order to make the most of tactile sensing, we believe that the biomimetic route, focusing particularly on the role of active control, can inspire technologies that will provide future robots with a sense of touch to parallel, or even surpass, that of animals. The BIOTACT Sensor described in this paper is we hope a useful step towards this longer term goal.

REFERENCES

[1] R. Bajcsy, "Active perception," *Proc. IEEE*, vol. 76, pp. 996–1005, 1988.

[2] S. J. Lederman and R. L. Klatzky, "Extracting object properties through haptic exploration," *Acta Psychol. (Amst)*, vol. 84, no. 1, pp. 29–40, 1993.

[3] T. Prescott, B. Mitchinson, and R. Grant, "Vibrissal behavior and function," *Scholarpedia*, 2011. [Online]. Available: http://www.scholarpedia.org/article/Vibrissal_behavior_and_function, to be published

[4] T. Prescott, M. Pearson, B. Mitchinson, J. Sullivan, and A. Pipe, "Whisking with robots from rat vibrissae to biomimetic technology for active touch," *IEEE Robot. Autom. Mag.*, vol. 16, no. 3, pp. 42–50, 2009.

[5] C. Fox, B. Mitchinson, M. Pearson, A. Pipe, and T. Prescott, "Contact type dependency of texture classification in a whiskered mobile robot," *Autonomous Robots*, vol. 26, pp. 223–239, 2009.

[6] A. S. Ahl, "The role of vibrissae in behavior – A status review," *Vet. Res. Commun.*, vol. 10, no. 4, pp. 245–268, 1986.

[7] B. Mitchinson, K. N. Gurney, P. Redgrave, C. Melhuish, A. G. Pipe, M. Pearson, I. Gilhespy, and T. J. Prescott, "Empirically inspired simulated electro-mechanical model of the rat mystacial follicle-sinus complex," *Proc. R Soc. London B Biol. Sci.*, vol. 271, no. 1556, pp. 2509–2516, Dec. 2004.

[8] D. N. Hill, R. Bermejo, H. P. Zeigler, and D. Kleinfeld, "Biomechanics of the vibrissa motor plant in rat: Rhythmic whisking consists of triphasic neuromuscular activity," *J. Neurosci.*, vol. 28, no. 13, pp. 3438–3455, 2008.

[9] M. Brecht, B. Preilowski, and M. M. Merzenich, "Functional architecture of the mystacial vibrissae," *Behav. Brain Res.*, vol. 84, no. 1-2, pp. 81–97, 1997.

[10] G. Carvell and D. Simons, "Biometric analyses of vibrissal tactile discrimination in the rat," *J. Neurosci.*, vol. 10, no. 8, pp. 2638–2648, 1990.
[11] B. Mitchinson, T.-S. Chan, J. Chambers, M. Pearson, M. Humphries, C. Fox, K. Gurney, and T. J. Prescott, "BRAHMS: Novel middleware for integrated systems computation," *Adv. Eng. Inform.*, vol. 24, no. 1, pp. 49–61, 2010.
[12] C. M. Williams and E. M. Kramer, "The advantages of a tapered whisker," *PLoS ONE*, vol. 5, no. 1, p. e8806, Jan. 2010.
[13] M. J. Hartmann, N. J. Johnson, R. B. Towal, and C. Assad, "Mechanical characteristics of rat vibrissae: Resonant frequencies and damping in isolated whiskers and in the awake behaving animal," *J. Neurosci.*, vol. 23, no. 16, pp. 6510–6519, Jul. 2003.
[14] P. Gao, R. Bermejo, and H. P. Zeigler, "Whisker deafferentation and rodent whisking patterns: Behavioral evidence for a central pattern generator," *J. Neurosci.*, vol. 21, no. 14, pp. 5374–5380, 2001.
[15] R. W. Berg and D. Kleinfeld, "Rhythmic whisking by rat: Retraction as well as protraction of the vibrissae is under active muscular control," *J Neurophysiol.*, vol. 89, no. 1, pp. 104–117, Jan. 2003.
[16] R. B. Towal and M. J. Hartmann, "Right-left asymmetries in the whisking behavior of rats anticipate head movements," *J Neurosci.*, vol. 26, no. 34, pp. 8838–46, 2006.
[17] B. Mitchinson, C. J. Martin, R. A. Grant, and T. J. Prescott, "Feedback control in active sensing: Rat exploratory whisking is modulated by environmental contact," *Royal Soc. Proc. B*, vol. 274, no. 1613, pp. 1035–1041, 2007.
[18] R. A. Grant, B. Mitchinson, C. W. Fox, and T. J. Prescott, "Active touch sensing in the rat: Anticipatory and regulatory control of whisker movements during surface exploration," *J. Neurophysiology*, vol. 101, pp. 862–874, 2009.
[19] B. Mitchinson, M. Pearson, C. Melhuish, and T. J. Prescott, "A model of sensorimotor co-ordination in the rat whisker system," in *Proc. 9th Int. Conf. Simulation of Adaptive Behaviour, From Animals to Animats 9*, 2006, pp. 77–88.
[20] M. J. Pearson, A. G. Pipe, C. Melhuish, B. Mitchinson, and T. J. Prescott, "Whiskerbot: A robotic active touch system modeled on the rat whisker sensory system," *Adaptive Beh.*, vol. 15, no. 3, pp. 223–240, 2007.
[21] M. J. Pearson, B. Mitchinson, J. Welsby, T. Pipe, and T. Prescott, "Scratchbot: Active tactile sensing in a whiskered mobile robot," in *From Animals to Animats 11*, S. Doncieux, B. Girard, A. Guillot, J. Hallam, J.-A. Meyer, and J.-B. Mouret, Eds. Berlin, Germany: Springer, 2010, vol. 6226, Lecture Notes in Computer Science, pp. 93–103.
[22] B. Mitchinson, M. J. Pearson, A. G. Pipe, and T. J. Prescott, "Biomimetic robots as scientific models: A view from the whisker tip," in *Neuromorphic and Brain-Based Robots*, J. Krichmar and H. Wagatsuma, Eds. Cambridge, MA: MIT Press, 2011, to be published.
[23] R. B. Towal and M. J. Z. Hartmann, "Variability in velocity profiles during free-air whisking behavior of unrestrained rats," *J. Neurophysiol.*, vol. 100, no. 2, pp. 740–752, 2008.
[24] M. Diamond, M. von Heimendahl, and E. Arabzadeh, "Whisker-mediated texture discrimination," *PLoS Biol.*, vol. 6, no. 8, 2008.
[25] F. Anjum, H. Turni, P. G. Mulder, J. van der Burg, and M. Brecht, "Tactile guidance of prey capture in Etruscan shrews," *Proc. Nat. Acad. Sci. U.S.A.*, vol. 103, no. 44, pp. 16 544–16 549, 2006.
[26] E. Ahissar and P. M. Knutsen, "Object localization with whiskers," *Biol. Cybern.*, vol. 98, no. 6, pp. 449–458, 2008.
[27] E. Guic-robles, G. Guajardo, and C. Valdivieso, "Rats can learn a roughness discrimination using only their vibrissal system," *Behavioral Brain Res.*, vol. 31, pp. 285–289, 1989.
[28] E. Guic-robles, W. M. Jenkins, and H. Bravo, "Vibrissal roughness discrimination is barrelcortex-dependent," *Behavioral Brain Res.*, vol. 48, no. 2, pp. 145–152, 1992.
[29] J. Hipp, E. Arabzadeh, E. Zorzin, J. Conradt, C. Kayser, M. E. Diamond, and P. Konig, "Texture signals in whisker vibrations," *J. Neurophysiol.*, vol. 95, no. 3, pp. 1792–9, 2006.
[30] J. Wolfe, D. N. Hill, S. Pahlavan, P. J. Drew, D. Kleinfeld, and D. E. Feldman, "Texture coding in the rat whisker system: Slip-stick versus differential resonance," *PLoS Biol.*, vol. 6, no. 8, p. e215, 2008.
[31] M. Evans, C. W. Fox, M. J. Pearson, and T. J. Prescott, "Tactile discrimination using template classifiers: Towards a model of feature extraction in mammalian vibrissal systems," in *Proc. 11th Int. Conf. Simulation of Adaptive Behavior*, 2010, pp. 178–187.
[32] M. Evans, C. W. Fox, M. J. Pearson, and T. J. Prescott, "Whisker-object contact speed affects radial distance estimation," in *Proc. IEEE Int. Conf. Robot. Biomimetics (ROBIO)*, 2010, pp. 720–725.
[33] N. F. Lepora, M. Evans, C. W. Fox, M. E. Diamond, K. N. Gurney, and T. J. Prescott, "Naive Bayes texture classification applied to whisker data from a moving robot," in *Proc. IEEE IJCNN*, Apr. 27, 2010, pp. 1–8.
[34] N. F. Lepora, M. Pearson, B. Mitchinson, M. Evans, C. Fox, T. Pipe, K. Gurney, and T. Prescott, "Naive Bayes novelty detection for a moving robot with whiskers," in *Proc. IEEE ROBIO'10*, 2010, pp. 131–136.
[35] M. Evans, C. W. Fox, M. J. Pearson, and T. J. Prescott, T. Kyriacou, U. Nehmzow, C. Melhuish, and M. Witkowski, Eds., "Spectral template based classification of robotic whisker sensor signals in a floor texture discrimination task," in *Proc. Towards Autonomous Robot. Syst., TAROS'09*, 2009, pp. 19–24.
[36] M. Kaneko, N. Kanayama, and T. Tsuji, "Active antenna for contact sensing," *IEEE Trans. Robot. Autom.*, vol. 14, no. 2, pp. 278–291, 1998.
[37] A. Lamperski, O. Loh, B. Kutscher, and N. Cowan, "Dynamical wall following for a wheeled robot using a passive tactile sensor," in *Proc. IEEE Int. Conf. Robot. Autom., ICRA'05*, 2005, pp. 3838–3843.
[38] P. Flandrin, F. Auger, and E. Chassande-Mottin, "Time-frequency reassignment: From principles to algorithms," in *Applications in Time Frequency Signal Processing*, A. Papreou-Suppappola, Ed. Boca Raton, FL: CRC Press, 2003, pp. 179–203.
[39] S. A. Anderson, M. J. Pearson, A. G. Pipe, T. J. Prescott, P. Dean, and J. Porrill, "Adaptive cancellation of self-generated sensory signals in a whisking robot," *IEEE Trans. Robotics*, pp. 1–12, Aug. 2010.

J. Charles Sullivan received the Ph.D. degree from the University of the West of England, Bristol, U.K., in 2001.

Currently, he is a Senior Lecturer at the University of the West of England and a member of the Bristol Robotics Laboratory. His research interests include dynamics modeling and analysis, finite-element analysis, evolutionary algorithms and optimization, biomechanics, and biomimetic design.

Ben Mitchinson received the Ph.D. degree in nonlinear learning machines from the University of Sheffield, Sheffiend, U.K., in 2002.

Currently, he is an ATLS Senior Postdoctoral Researcher. His research interests include the vibrissal sensory system, and bioinspired information processing and robotics.

Martin J. Pearson received the B.Eng. degree in electrical and electronics engineering from the University of Manchester, Manchester, U.K., the MSc. degree in advanced technologies in electronics and the Ph.D. degree in 2008 from the University of the West of England, Bristol, U.K.

Currently, he is a Research Fellow at the Bristol Robotics Laboratory with research interests in bio-inspired robotics, neural control, and reconfigurable computing.

Mat Evans received the B.Sc. degree in psychology and the M.Sc. degree in computational and systems neuroscience from the University of Sheffield, Sheffield, U.K. Currently, he is working towards the Ph.D. degree in whisker-based tactile perception with the Adaptive Behaviour Research Group, Department of Psychology, University of Sheffield.

His research interests include active sensing, encoding of (tactile) stimuli, sensory-motor interaction, and embedded models thereof.

Nathan F. Lepora received the B.A. degree in mathematics and the Ph.D. degree in theoretical physics from the University of Cambridge, Cambridge, U.K.

He was a Research Fellow with Kings College, University of Cambridge for four years. Currently, he is a Research Associate with the Adaptive Behavior Research Group, Department of Psychology, University of Sheffield. His research interests include various topics between the interface of the physical and life sciences.

Charles W. Fox received the M.A. degree in computer science from the University of Cambridge, Cambridge, U.K., the M.Sc. degree in cognitive science from the University of Edinburgh, Edinburgh, U.K., and the D.Phil. degree in engineering from the University of Oxford, Oxford, U.K.

He was a Quantitative Hedge Fund Analyst at Algometrics Ltd. and Vantage Investment Advisory Ltd. for two years. Currently, he is a Research Associate with the Adaptive Behavior Research Group, Department of Psychology, University of Sheffield, and a co-investigator on the EU BIOTACT and EFAA projects. His research interests include applying machine learning techniques to neuroscience.

Chris Melhuish is Director of the Bristol Robotics Laboratory, a partnership between the University of Bristol and the University of the West of England, Bristol, U.K. His research interests include collective mobile robotics, robot-human interaction, neuro-inspired systems, and energy autonomy in robots. In addition to his Chair at the University of the West of England in Intelligent Autonomous Systems, he also holds the Chair in Robotics and Autonomous Systems, University of Bristol.

Prof. Melhuish is a Fellow of the British Computer Society, Fellow of the Institution of Engineering Technology, and is a Chartered Engineer.

Tony J. Prescott received the the M.A. degree in psychology from the University of Edinburgh, Edinburgh, U.K., the M.Sc. degree in applied A.I. from the University of Aberdeen, Aberdeen, U.K., and the Ph.D. degree in machine learning from the University of Sheffield, Sheffield, U.K.

Currently, he is a Professor of Cognitive Neuroscience at the University of Sheffield, where he directs the Active Touch Laboratory and co-directs the Adaptive Behavior Research Group. He is also the coordinator of the EU Framework 7 BIOTACT project. His research interests are focused on understanding the functional architecture of the vertebrate brain using techniques in computational neuroscience, robotics, and neuroethology.